Pressure-Induced Postsynthetic Cluster Anion Substitution in a MIL-53 Topology Scandium Metal-Organic Framework

Alexander J. R. Thom,[a] Gemma F. Turner,[b] Zachary H. Davis,[c] Martin R. Ward,[d] Ignas Pakamorė,[a] Claire L. Hobday,[e] David R. Allan,[f] Mark R. Warren,[f] Iain D. H. Oswald,[d] Russell E. Morris,[c] Stephen A. Moggach,[b*] Sharon E. Ashbrook[c*] and Ross S. Forgan[a*]

[a]WestCHEM School of Chemistry, University of Glasgow, Joseph Black Building, University Avenue, Glasgow G12 8QQ, UK.
Email: ross.forgan@glasgow.ac.uk

[b]School of Molecular Sciences, The University of Western Australia, 35 Stirling Highway, Crawley, Perth, Western Australia, 6009, Australia.
Email: stephen.moggach@uwa.edu.au

[c]EaStCHEM School of Chemistry and Centre of Magnetic Resonance, University of St Andrews, St Andrews KY16 9ST, UK.
Email: sema@st-andrews.ac.uk

[d]Strathclyde Institute of Pharmacy & Biomedical Sciences (SIPBS), University of Strathclyde, 161 Cathedral Street, Glasgow, G4 0RE, UK.

[e]EaStCHEM School of Chemistry and Centre for Science at Extreme Conditions, The University of Edinburgh, King's Buildings, David Brewster Road, Edinburgh EH9 3FJ, UK.

[f]Diamond Light Source Ltd, Harwell Science and Innovation Campus, Didcot, Oxfordshire OX11 0DE, UK.

Abstract

Postsynthetic modification of metal-organic frameworks (MOFs) has proven a hugely powerful tool to tune physical properties and introduce functionality, by exploiting reactive sites on both the MOF linkers and their inorganic secondary building units (SBUs), and so has facilitated a wide range of applications. Studies into the reactivity of MOF SBUs have focussed solely on removal of neutral coordinating solvents, or direct exchange of linkers such as carboxylates, despite the prevalence of ancillary charge-balancing oxide and hydroxide ligands found in many SBUs. Herein, we show that the μ_2-OH ligands in the MIL-53 topology Sc MOF, GUF-1, are labile, and can be substituted for μ_2-OCH_3 units through reaction with pore-bound methanol molecules in a very rare example of pressure-induced postsynthetic modification. Using comprehensive solid-state NMR spectroscopic analysis, we show an order of magnitude increase in this cluster anion substitution process after exposing bulk samples suspended in methanol to a pressure of 0.8 GPa in a large volume press. Additionally, single crystals compressed in diamond anvil cells with methanol as the pressure-transmitting medium have enabled full structural characterisation of the process across a range of pressures, leading to a quantitative single-crystal to single-crystal conversion at 4.98 GPa. This unexpected SBU reactivity – in this case chemisorption of methanol – has implications across a range of MOF chemistry, from activation of small molecules for heterogeneous catalysis to chemical stability, and we expect cluster anion substitution to be developed into a highly convenient novel method for modifying the internal pore surface and chemistry of a range of porous materials.

Introduction

Metal-organic frameworks (MOFs), coordination polymers wherein metal ions/clusters are connected by multitopic linkers into network structures,[1] are being extensively investigated for a number of applications based around the chemistry of the inorganic secondary building unit (SBU). Kinetically labile bonds between metals and ligands can allow access to coordinatively unsaturated metal sites[2-4] that endow MOFs with catalytic properties,[5-7] enhance their interactions with sorbates such as H_2,[8-11] and offer potential sensing mechanisms.[12-14] Dynamic SBU solvent substitution can facilitate structural flexibility[15,16] and metal-ion exchange,[17,18] while also offering routes to pore functionalisation through linker exchange,[18-22] linker incorporation/grafting,[23-26] and defect substitution.[27-33] Coordinative exchange reactions may also be responsible for MOF degradation, for example through hydrolysis.[34] To date, most studies on such reactions within MOFs focus on either binding and removal of neutral solvent molecules,[35] or direct exchange of carboxylate and/or pyridyl-based ligands, despite the fact that a significant number of commonly observed SBUs contain bridging oxo or hydroxo ligands.[36] Some of us have recently developed solid-state (and in particular ^{17}O) NMR spectroscopy as a valuable analytical tool to study structural and chemical changes in microporous materials such as MOFs and zeolites.[37-40] In doing so, we have shown that the bridging μ_2-OH ligand in the one-dimensional chain SBU of MIL-53(Sc), $[ScOH(BDC)]_n$ (BDC = 1,4-benzenedicarboxylate), is labile, observing up to 25% enrichment with ^{17}O by reaction with $H_2{}^{17}O$ (90% ^{17}O) under hydrothermal conditions (200 °C, 72 h).[38] Allied to the fact that MIL-53 analogues are known with alternative anionic[41-43] and neutral[44-46] bridging ligands, this suggests a rich potential reactivity at this particular SBU.

Herein, we report the pressure-induced reactivity of the SBU of the Sc MOF GUF-1 (GUF = Glasgow University Framework), where the 4,4′-(ethyne-1,2-diyl)dibenzoate (EDB^{2-}) ligand links one-dimensional ScOH SBUs into a two-fold interpenetrated net with the MIL-53 topology and overall formula $[ScOH(EDB)]_n$.[47] Using high-pressure techniques alongside solid-state NMR spectroscopy, we show that up to 17(2)% of bridging μ_2-OH ligands can be replaced by bridging μ_2-OCH_3 units in the bulk phase by reaction with methanol at 0.8 GPa in a large volume press, with conversions of up to 98(4)% in a single crystal pressurised to 4.98 GPa in methanol in a diamond anvil cell (DAC) observed by single crystal X-ray diffraction. This is at least an order of magnitude higher than analogous reactivity under ambient conditions, and represents a rare example of pressure-induced postsynthetic modification of MOFs[48] with significant implications for their activation with methanol, and processing and shaping for application.

Results and Discussion

We recently reported the synthesis, structure, and excellent H_2 storage capacity of GUF-1.[47] As its interpenetration results in limited breathing in comparison to non-interpenetrated MIL-53 topology MOFs,[49,50] allied to the fact that it has a potentially flexible EDB^{2-} linker, we sought to characterise its structural response to pressure using high-pressure single crystal X-ray diffraction in a DAC. This approach[51] has previously allowed us and others to characterise mechanical compliance of a range of MOFs,[52-57] as well as to investigate the structural basis of spectroscopic responses to pressure and different guests.[58,59] Single crystals of GUF-1-(HCl) were prepared according to our previously reported HCl modulated solvothermal synthesis in *N*,*N*-dimethylformamide (DMF),[47] and transferred into fresh DMF for storage (see supplementary information, Section S2). Under ambient conditions, GUF-1 forms pale pink cuboidal crystals in the orthorhombic space group, *Cmme*. One-dimensional chains of corner-sharing ScO_6 octahedra extend along the crystallographic *a*-axis (Figure 1a). The chains are tethered at the Sc^{III} centres by bridging EDB^{2-} ligands to form a wine-rack net in the *bc* plane of the unit cell (Figure 1b), which is two-fold interpenetrated and perforated by rhombic, one-dimensional channels that run parallel to the ScO_6 chains down the *a*-axis (Figure 1c). We have previously quantified the flexibility of the material by measuring the internal angles of the rhombic pore, Ψ and Φ (Figure 1b). There are two types of chemically distinct channels. One is decorated by μ_2-OH groups at the shared corners of ScO_6 pairs, and contains two DMF molecules from the crystallisation solvent per unit formula, with a hydrogen bonding interaction between the formyl group of the DMF and the H atom of the bridging hydroxide (O···O = 2.89(2) Å).[47] The second channel is vacant upon synthesis, with a solvent accessible volume of 270 $Å^3$ (probe radius = 1.2 Å, grid spacing = 0.7 Å, Mercury, CSD). [60]

A single crystal of GUF-1-(HCl) was transferred from DMF storage and compressed in a modified Merrill-Bassett DAC[61] using methanol (CH_3OH) as the pressure-transmitting medium; CH_3OH is a commonly used solvent which is small enough to infiltrate the framework pores and remains liquid to high pressures (see supplementary information, Section S3). Compression was followed by *in situ* single crystal X-ray diffraction up to 4.98 GPa. A crystal of GUF-1-(HCl) was also compressed in a non-penetrating medium of Fluorinert® FC-70 to examine its flexibility under direct pressure. However, the crystal became polycrystalline at the initial loading pressure of 0.1 GPa, so no further structural analysis was performed. Crystallographic and structural data are given in Table 1 and supplementary information, Tables S2 and S3.

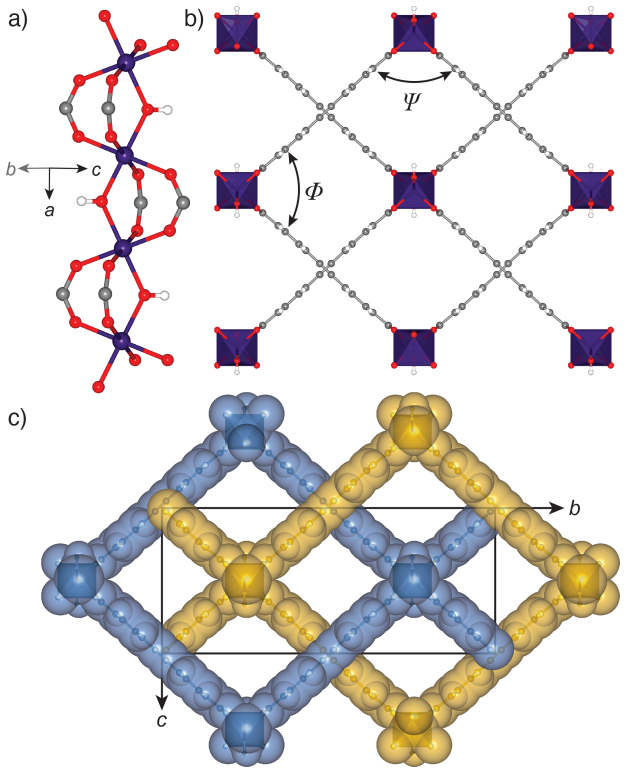

Figure 1. Solid state-structure of GUF-1-(HCl). **a**) Infinite chain SBU of ScO_6 octahedra with bridging μ_2-OH ligands that runs down the crystallographic *a*-axis. **b**) Fragment of the packing structure viewed down the crystallographic *a*-axis, with interior pore angles Ψ and Φ labelled. **c**) Two-fold interpenetrated packing structure with individual nets coloured blue and yellow, and the unit cell overlaid. Where applicable, atoms are coloured Sc: purple; C: grey; O: red; H: yellow. H atoms and pore-bound DMF in parts **b**) and **c**) are omitted for clarity. Reproduced from CSD deposition 2095589.[47]

Compression of GUF-1-(HCl) in CH_3OH between ambient pressure and 4.98 GPa causes the unit cell volume to decrease by 158.9(9) Å (–7.0%) (Figure 2a, Table 1). The compression occurs in two stages, marked by a change in the compressibility of the crystal at 0.71 GPa. Initial compression of native GUF-1 between ambient pressure and 0.47 GPa causes the unit cell volume to *increase* by 55.3(9) $Å^3$ (+2.4%) with the associated change in the channel shape indicated by an increase in ψ, the hinge angle of the framework defined as the angle between intersecting EDB^{2-} linkers[47] (Figure 2b, Table 1). Compression of native GUF-1 promotes adsorption of CH_3OH into the previously vacant channels at 0.23 GPa, expanding the structure (Figure 2c). Subsequently, postsynthetic modification occurs suddenly at a critical pressure of 0.71 GPa, (Figure 2d) and involves partial exchange of the μ_2-OH ligand for a bridging methoxide group, μ_2-OCH_3, in a single-crystal-to-single-crystal reaction with retention of the *Cmme* symmetry. The high-pressure phase observed between 0.71 GPa and 4.98 GPa (Figure 2e) therefore corresponds to a postsynthetically modified framework, denoted as GUF-1-OCH_3. At 0.71 GPa, conversion from GUF-1 to GUF-1-OCH_3 is

measured to be 33(3)%, according to the refined crystallographic occupancy of the C atom of the methyl group.

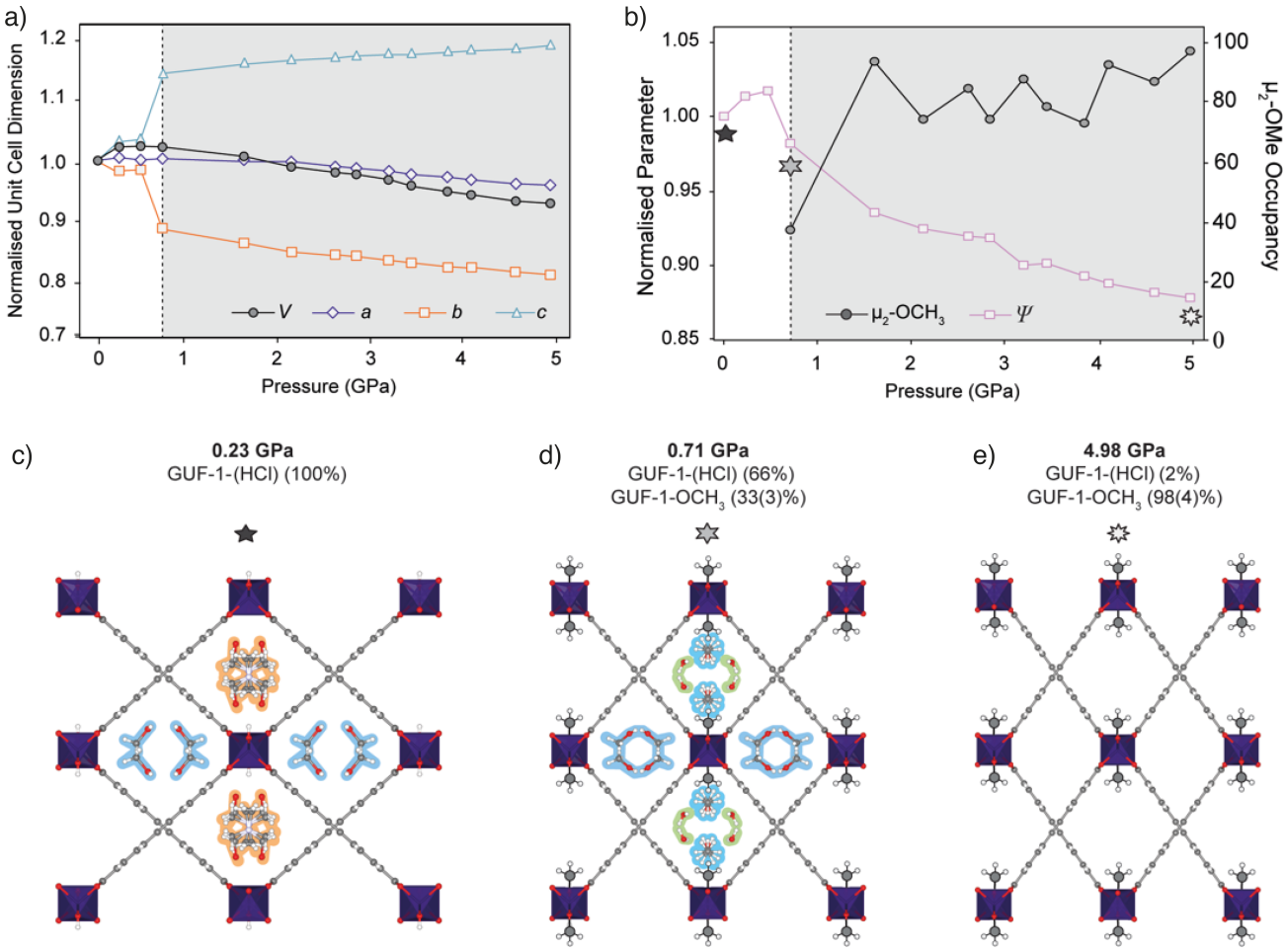

Figure 2. a) Unit cell volume (black) and normalised unit cell axis lengths (*a* – purple diamonds, *b* – orange squares, *c* – blue triangles) of GUF-1-(HCl) (white region) and GUF-1-OCH_3 (shaded region) during hydrostatic compression in CH_3OH. Error bars are within the data markers. **b)** Plot of the refined occupancy of the exchanged μ_2-OCH_3 bridge (grey circles) and Ψ hinge angle (pink squares) during compression. The stars correspond to individual structures shown in **c)-e)**. **c**) Crystal structure of GUF-1-(HCl) at 0.23 GPa viewed along the crystallographic *a*-axis, showing disordered DMF (highlighted in orange) and CH_3OH (highlighted in blue) in the pores. **d**) Crystal structure of the post-synthetically modified framework, GUF-1-OCH_3, at 0.71 GPa with the CH_3 groups enhanced for clarity. Adsorbed water in the pores is highlighted in green. At this pressure, 33(3)% of the μ_2-OH groups have been exchanged for μ_2-OCH_3. **e**) Structure of GUF-1-OCH_3 at 4.98 GPa, where 98(4)% of the μ_2-OH groups have been exchanged for μ_2-OCH_3 and the wine-rack structure is compressed.

Table 1. Unit cell axes and refined crystallographic occupancy of μ_2-OCH_3 for GUF-1 and GUF-1-OCH_3 during hydrostatic compression in a pressure transmitting medium of CH_3OH. All structures are in the space group *Cmme*.

P **/ GPa**	***a*** **/ Å**	***b*** **/ Å**	***c*** **/ Å**	***V*** **/ Å^3**	**μ_2-OCH_3 occ. / %**
0.00[a]	7.3054 (5)	26.5207 (17)	11.7550 (9)	2277.5 (5)	0.00
0.23	7.3533 (9)	26.584 (12)	11.879 (4)	2322.2 (14)	0.00
0.47	7.3205 (15)	26.609 (5)	11.922 (2)	2322.2 (8)	0.00
0.71	7.3445 (19)	23.984 (3)	13.1770 (13)	2321.1 (7)	0.33(3)
1.61	7.3293 (16)	23.332 (3)	13.3614 (11)	2284.9 (6)	0.93(4)
2.13	7.290 (3)	22.957 (4)	13.4286 (14)	2247.4 (9)	0.69(5)
2.61	7.241 (4)	22.814 (7)	13.473 (3)	2225.6 (14)	0.82(5)
2.84	7.213 (2)	22.789 (3)	13.4966 (13)	2218.6 (7)	0.72(4)
3.20	7.180 (2)	22.587 (4)	13.5541 (13)	2198.2 (7)	0.85(4)
3.45	7.1429 (17)	22.463 (5)	13.5504 (12)	2174.2 (7)	0.78(5)
3.85	7.1069 (17)	22.297 (4)	13.5859 (16)	2152.8 (7)	0.68(4)
4.11	7.0769 (18)	22.232 (6)	13.613 (15)	2141.7 (6)	0.90(4)
4.60	7.0380 (14)	22.061 (7)	13.652 (2)	2119.8 (8)	0.85(4)
4.98	7.0142 (12)	21.941 (7)	13.6972 (19)	2108.0 (8)	0.98(4)

[a]Separate crystal, data collection at ambient pressure at 273 K.

Postsynthetic cluster anion substitution is clearly facilitated by the pressure-induced intrusion of CH_3OH from the hydrostatic medium into the framework channels. At 0.71 GPa, the pressure is sufficient to promote exchange of the DMF in the μ_2-OH decorated channel for CH_3OH and H_2O (Figure 2d), which brings the reactant CH_3OH in close proximity to the μ_2-OH sites, (O···O = 5.2(3) Å), likely promoting the postsynthetic ligand exchange. The subsequent identification of adsorbed H_2O could result from this being the by-product of the μ_2-OH for μ_2-OCH_3 exchange or, alternatively, it may originate from residual moisture in the pressure transmitting medium. The CH_3OH is adsorbed at two independent sites near the centre of the channel, with occupancies of ~20% at 0.71 GPa, one of which is disordered over a mirror plane, while H_2O is located in two

equivalent sites near the corner of the rhombic channel, with an occupancy of ~34%, which corresponds closely to the percentage of OH exchange at this pressure, 33(3)%. Above 0.71 GPa, the adsorbate became highly disordered and so was modelled using the SQUEEZE[62] algorithm in PLATON.[63]

The mechanism of the postsynthetic cluster anion substitution process cannot be ascertained from the crystal structure, although it is possible that the guest exchange and ligand exchange are concerted, accounting for the high pressure required to facilitate the reaction. Intuitively, ligand exchange is likely to be an associative process involving coordination of methanol and breaking of one of the Sc-OH bonds, maintaining the overall six-coordinate environment around the Sc^{III} ions, followed by proton transfer from methanol to hydroxide, water dissociation, and subsequent coordination to the now bridging μ_2-OCH_3 unit. Confinement of H_2O in the channel may promote the reverse ligand exchange, which would account for the partial conversion of GUF-1 to GUF-1-OCH_3 at 0.71 GPa. The possible equilibrium between μ_2-OH, μ_2-OCH_3, H_2O and CH_3OH may create a pressure dependence on the conversion to GUF-1-OCH_3, which shows a fluctuating increase from 33(3)% to 98(4)% between 0.71 GPa and 4.98 GPa, with pressure-induced intrusion of CH_3OH into the channels favouring the forward, μ_2-OH to μ_2-OCH_3, ligand exchange (Figure 2b, Table 1).

The μ_2-OH to μ_2-OCH_3 ligand exchange is associated with a decrease in the porosity of the framework and compression of the wine-rack structure. In GUF-1-OCH_3, the methyl groups of the μ_2-OCH_3 ligands protrude into the channel, decreasing the pore volume by 39 $Å^3$ (–13.1%) between 0.47 GPa and 0.71 GPa (Figure 3 and Table S3), and increasing its hydrophobicity. In addition, the protruding methyl groups form intra-framework CH···π interactions with pairs of aromatic rings from the $EDB^{2–}$ ligands across the rhombic channel (CH···π = 4.83(3) Å at 0.71 GPa, Figure 3), causing the channel to become compressed in width and extended in height (Table S3), facilitated by the hinging motion of the $EDB^{2–}$ linkers about the Sc^{III} centres. Upon formation of GUF-1-OCH_3, the hinge angle, Ψ, decreases from 97.41(3)° to 94.30(2)°, compressing the wine-rack structure. This is associated with a sudden contraction of the *b*-axis by 2.625(6) Å (–9.9%) and extension of the *c*-axis by 1.255(2) Å (+10.5%) between 0.47 GPa and 0.71 GPa, while the *a*-axis and cell volume remain largely unchanged (Table 1). This type of topological compression and associated negative linear compressibility are common to MIL-type frameworks[64-67] and, in GUF-1-OCH_3, results from both the formation of new intra-framework interactions and from the application of hydrostatic pressure. Upon further compression of GUF-1-OCH_3 from 0.71 GPa to 4.98 GPa, ψ gradually decreases by 3.75(4)° (–4.0%, Figure 2b, Table S3). No such behaviour is

observed in the native framework, GUF-1-(HCl), up to 0.47 GPa due to the initial intrusion of CH_3OH into the channels, which limits the framework flexibility. As the methoxide-decorated channel is compressed between 0.71 GPa and 4.98 GPa, the intraframework CH···π interactions shorten by 0.55(6) Å (-11.4%), which may help to stabilise the more contracted structure.

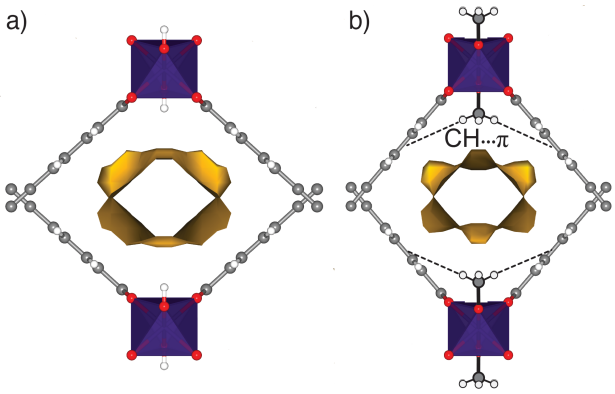

Figure 3. Fragments of **a)** GUF-1-(HCl) (ambient pressure) and **b)** GUF-1-OCH_3 (0.71 GPa) showing the solvent accessible volume (yellow). In GUF-1-OCH_3, intraframework CH···π interactions are shown as dashed lines.

This cluster anion substitution reaction, in effect pressure-induced chemisorption of methanol, is highly unusual in metal-organic frameworks, although the experimental set-up using the DAC only allows probing of an individual crystal. As we have previously used solid-state NMR spectroscopy to successfully monitor exchange of μ_2-OH ligands with isotopically enriched water in the related MOF MIL-53(Sc),[38] we again turned to this technique to determine if the bulk reactivity mirrored that observed in the single crystal. Large-scale samples of the MOF were prepared by acetic acid modulated synthesis to yield GUF-1-(AcOH) and the as-synthesised materials exchanged with either fresh DMF as a control sample, or different isotopologues of methanol; natural abundance CH_3OH, CD_3OD (99% ^2H), and $^{13}CH_3OH$ (99% ^{13}C). A large volume press was used to apply pressure to the samples (see supplementary information, Section S4). Each suspension was individually transferred to a sample chamber comprising a 60 mm length of Teflon tubing (ID 8 mm, OD 10 mm) sealed with Teflon caps and Teflon tape. The sample capsule was inserted into a large volume press assembly and a load of 7 tonnes was applied (equivalent pressure = 0.8 GPa).[68] The samples were held at elevated pressure for a period of 16 h at room temperature (*ca.* 20 °C). For all tested samples, the load on the sample had decreased to ~6-6.5 tonnes (pressure = 0.69 – 0.75 GPa) indicating a decrease in sample pressure over the 16 h period. This is frequently observed in other systems and hence is due to a mechanical effect rather than changes to the sample. After this time, the sample was returned to atmospheric pressure over a period of 10 minutes and

recovered as a suspension. Control experiments were carried out on identical samples that were exchanged in methanol at ambient pressure for the same time period. The samples are named GUF-1-(solv)-*X*, where solv = DMF or the methanol isotopologue used, and *X* = *am* (ambient) or *P* (pressurised to 0.8 GPa) to denote the pressure used for postsynthetic exchange (see supplementary information, Table S1).

Solid-state NMR spectroscopy was then employed to further investigate the nature of the cluster anion substitution process using ^{13}C, ^{1}H and ^{2}H magic angle spinning (MAS) NMR experiments (see supplementary information, Section S5). Assignments of the signals from the linker carbon environments are based on ^{13}C NMR experiments performed on GUF-1-(DMF)-*am* (see supplementary information, Section 5.1, which includes the atom labelling scheme). No resonances corresponding to acetic acid, or acetate acting as a cluster-capping defect were observed before or after exchange with DMF. Initial ^{13}C MAS and cross polarisation (CP) MAS NMR spectra (see supplementary information, Section 5.2) acquired for a sample exchanged with unenriched methanol at ambient pressure – GUF-1-(CH_3OH)-*am* – show five resonances corresponding to the MOF linker at δ = 170 (C1, carboxyl carbon), 134 (C2), 132 (C3 and C4), 127 (C5), and 96 ppm (C6, alkyne carbon), as well as three resonances arising from the presence of DMF (δ = 161, 35 and 30 ppm). Alongside these peaks is a small additional resonance at 56 ppm, a typical δ_{iso} value for the ^{13}C nucleus of a OCH_3 group. This peak remains following calcination of the MOF at 140 °C, 10^{-4} Torr for 48 hours, indicating it arises from framework bound OCH_3 rather than free CH_3OH within the MOF pores. However, the intensity of this signal is low, and accurate information on the relative percentage of unenriched CH_3OH exchange taking place within the framework cannot be determined easily from these ^{13}C NMR spectra.

Repeating the methanol exchange process with $^{13}CH_3OH$ (99% ^{13}C) enables ^{13}C NMR spectra to be acquired with an improved signal-to-noise ratio. This process was performed on two samples of GUF-1-(AcOH), one exchanged under ambient pressure conditions – GUF-1-($^{13}CH_3OH$)-*am* – and a second which had been pressurised to 0.8 GPa in the large volume press, GUF-1-($^{13}CH_3OH$)-*P*. Both materials were stored in their $^{13}CH_3OH$ solvent for 6 further days after pressurisation, prior to filtering and packing in MAS NMR rotors. ^{13}C and ^{1}H MAS NMR spectra were acquired on the freshly filtered materials, and subsequently after calcination at 140 °C, 10^{-4} Torr for 48 h. The ^{13}C MAS NMR spectra for the materials before and after calcination are shown in Figures 4a and 4b, while ^{13}C CP MAS and ^{1}H MAS NMR spectra are provided in the supplementary information, Section 5.3. In order to acquire a quantitative ^{13}C MAS NMR spectrum, T_1 relaxation measurements were carried out on GUF-1-($^{13}CH_3OH$)-*am* using a saturation recovery experiment,

which indicated the alkyne carbon had the slowest relaxation (with T_1 values of 10 and 12 s for the post-soaking and calcined forms, respectively) and thus a recycle interval of 2 minutes was utilised for every ^{13}C MAS NMR spectrum. The ^{13}C MAS NMR spectrum of the GUF-1-($^{13}CH_3OH$)-*am* (Figure 4a) shows significant enhancement of the resonance at 56 ppm, providing further evidence that this peak relates to the exchanged μ_2-OCH_3. Fitting and integrating the peaks in the spectrum, including spinning sidebands, indicates 2.2(2)% of the hydroxyl groups in the framework have been replaced with μ_2-OCH_3 following the ambient pressure exchange step. After calcination this value decreases to 1.6(3)%, suggesting a very small portion of free $^{13}CH_3OH$ is still present in the material. Additional resonances arise in the ^{13}C MAS NMR spectrum between 10 – 50 ppm when the material is exchanged with $^{13}CH_3OH$. It is believed that these peaks correspond to a minor impurity in the material, present at 2.3% (*w/w*), but are only observable when $^{13}CH_3OH$ is used, indicating the impurity originates from the CH_3OH solvent. A more detailed discussion of the possible nature of these signals is included in the supplementary information, Section 5.3. For the sample prepared under high pressure, GUF-1-($^{13}CH_3OH$)-*P*, the percentage of μ_2-OCH_3 exchange increases significantly to 20(4)%, decreasing slightly to 17(2)% following calcination (Figure 4b), confirming the significant effect of pressure in enhancing ligand exchange by an order of magnitude. These values correspond reasonably well with the 33(3)% μ_2-OCH_3 exchange observed using crystallography at 0.71 GPa. Powder X-ray diffraction analysis of the samples recovered following the solid-state NMR spectroscopy shows that the MOFs remain intact after the bulk scale pressurisation, with some minor differences in relative peak intensities apparent after calcination (see supplementary information, Section S6).

To provide additional evidence of μ_2-OCH_3 binding to the GUF-1 framework, ^2H MAS NMR spectra of materials exchanged using CD_3OD (99% ^2H) were acquired to investigate any limitations on free rotation of methanol through measurement of the ^2H quadrupolar coupling constant, C_Q. In general, for ^2H in a molecule which can rotate isotropically, as in solution, a C_Q value of 0 would be observed (*i.e.,* the anisotropic quadrupolar interaction would be completely removed). Larger values of C_Q indicate restricted motion of the molecule, for example if μ_2-OCH_3 was bound to the MOF. The ^2H MAS NMR spectra of the calcined frameworks in Figures 4c and 4d, GUF-1-(CD_3OD)-*am* and GUF-1-(CD_3OD)-*P*, respectively, show two resonances at 3.9 and −0.5 ppm (insets), corresponding to deuterated μ_2-OCD_3 and the previously mentioned minor impurity (see supplementary information, Section 5.3), respectively. Fitting of the resonance at 3.9 ppm gives a C_Q value of 46(3) kHz for the framework exchanged under ambient conditions and 48(3) kHz when exchange is carried out under higher pressure. Both fittings provide an η_Q value of 0.0(2) confirming an axially symmetric averaged electric field gradient tensor, as expected for a C_3

rotation. This provides further evidence that the resonance at 3.9 ppm corresponds to μ_2-OCH_3 that is bound to the MOF at the SBU rather than present as free CH_3OH within the framework pores.

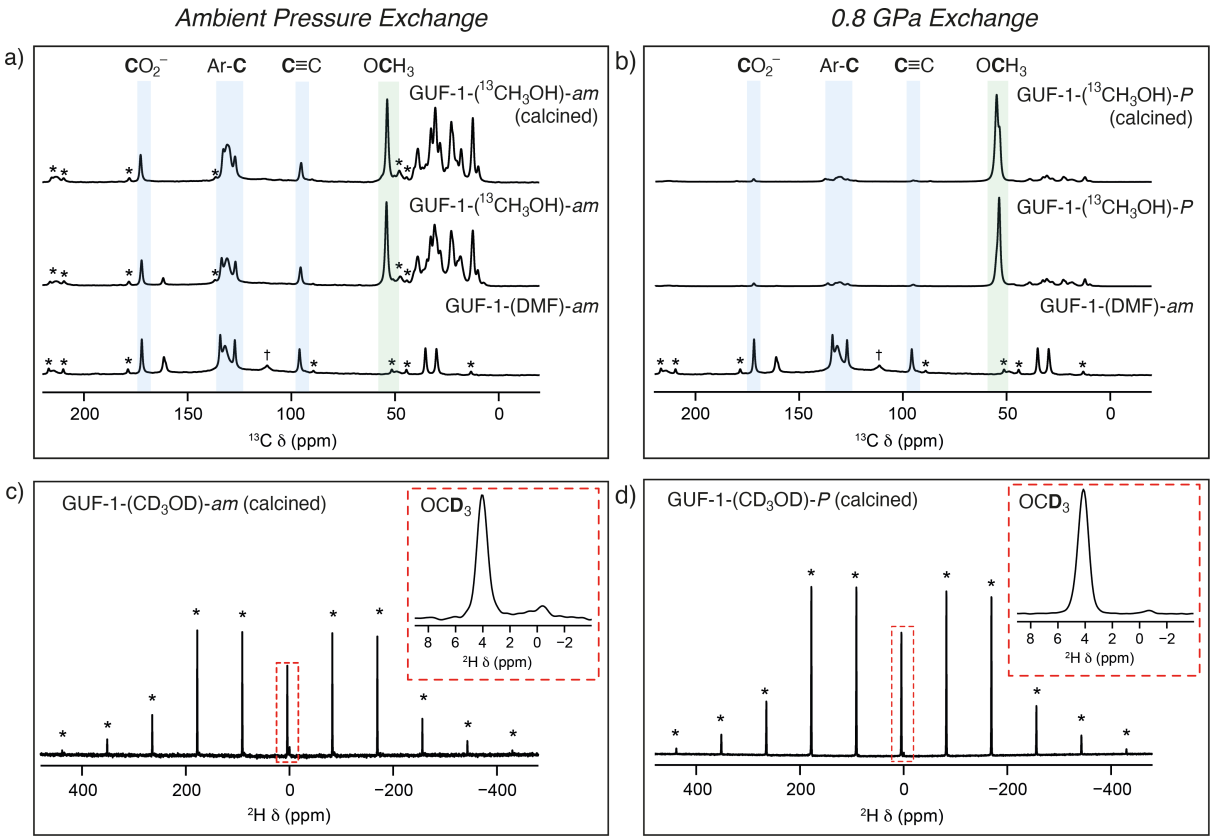

Figure 4. Top: Comparative ^{13}C (14.1 T, 12.5 kHz) MAS NMR spectra of GUF-1-(DMF)-*am* before and after soaking in $^{13}CH_3OH$ and calcination at **a)** ambient pressure (GUF-1-($^{13}CH_3OH$)-*am*), and **b)** at 0.8 GPa in the large volume press (GUF-1-($^{13}CH_3OH$)-*P*). Resonances shaded in blue correspond to carbon atoms of the EDB^{2-} linker, and the resonances shaded green to the OCH_3 group coordinated to the SBU (56 ppm). Resonances for ^{13}C nuclei of DMF are visible in the spectrum of GUF-1-(DMF)-*am* at 30, 35, and 161 ppm. Resonances between 10-50 ppm correspond to a minor impurity introduced by the $^{13}CH_3OH$ (see supporting information). Bottom: ^{2}H (14.1 T, 8 kHz) MAS NMR spectra of **c)** GUF-1-(CD_3OD)-*am* and **d)** GUF-1-(CD_3OD)-*P*, with the resonances assigned to the OCD_3 group at 4 ppm shown in inserts. Dagger (†) denotes a signal arising from a PTFE 4 mm MAS NMR rotor insert. Asterisks (*) denote spinning sidebands.

Conclusions

In summary, we have demonstrated that the bridging μ_2-OH ligands in the MIL-53 topology Sc^{III} MOF GUF-1 can be exchanged for μ_2-OCH_3 ligands through pressure-induced reaction with pore-bound methanol in a process we have termed cluster anion substitution. Up to 98(4)% of the μ_2-OH

groups were seen to exchange crystallographically at 4.98 GPa in a single crystal pressurised in a diamond anvil cell, while solid-state NMR spectroscopy showed 17(2)% exchange in bulk samples subjected to 0.8 GPa in a large volume press, an order of magnitude greater than the 1.6(3)% exchange observed for samples soaked in methanol under ambient conditions. These findings provide further evidence of the lability of bridging hydroxo ligands commonly found in MOF SBUs, and suggest that CH_3OH activation of MOFs should be carefully monitored for unintentional reactivity and chemisorption of the solvent. The presumably associative ligand exchange mechanism could be a proxy not only for solvent-induced structural breakdown of MOFs – for example certain Zr MOFs containing μ_2-OH ligands at their SBUs are known to be sensitive to CH_3OH[69-71] – but also a potential mechanism for small molecule activation, as similar bridging methoxide units at the SBUs of related MOFs have been implicated in catalytic mechanisms.[72] In addition, the presence of μ_2-OCH_3 in the SBUs could explain changes in physical properties observed when related MIL-53 analogues are directly synthesised in CH_3OH.[73,74] Our bulk scale pressure measurements identified a low level (~2%) pore-located impurity in the samples, which we have not currently identified, but whose isotopic enrichment confirms its origin in the $^{13}CH_3OH$ used to induce reactivity. Future work will seek to identify this material and exploit transient alkoxide coordination for catalytic reactions.

Acknowledgements

RSF thanks the Royal Society for receipt of a URF, EPSRC (EP/N509668/1), and the University of Glasgow for funding. IDHO and MRW thank EPSRC for funding (EP/015401/1). We acknowledge Diamond Light Source for time on I19-2 under proposal CY24020. ZHD thanks the ERC (Advanced Grant 787073 ADOR) for studentship funding. CLH thanks UKRI for a Future Leaders Fellowship (MR/V026070/1) and the University of Edinburgh for a Chancellor's Fellowship. SAM acknowledges the support of the Australian Research Council (ARC) from a Future Fellowship (FT200100243) and Discovery Project (DP 220103690).

Author Contributions

RSF and SAM conceived the project. AJRT synthesised all materials, and carried out all postsynthetic modifications and lab scale characterisation. AJRT, GFT, IP, CLH, DRA and MRW (Warren) carried out high-pressure single crystal X-ray diffraction measurements at Diamond Light Source, and GFT and SAM analysed the data. MRW (Ward) and IDHO carried out bulk scale pressurisation experiments in the high-volume press. ZHD carried out solid-state NMR

spectroscopic experiments and analysed the data with REM and SEA. All authors contributed to the preparation of the manuscript, which was initially drafted by AJRT, RSF, GFT, SAM, ZHF, and SEA.

References

1. Furukawa, H., Cordova, K.E., O'Keeffe, M., and Yaghi, O.M. (2013). The Chemistry and Applications of Metal-Organic Frameworks. Science *341*, 1230444. 10.1126/science.1230444.
2. Bae, J., Choi, J.S., Hwang, S., Yun, W.S., Song, D., Lee, J., and Jeong, N.C. (2017). Multiple Coordination Exchanges for Room-Temperature Activation of Open-Metal Sites in Metal–Organic Frameworks. ACS Applied Materials & Interfaces *9*, 24743-24752. 10.1021/acsami.7b07299.
3. Kökçam-Demir, Ü., Goldman, A., Esrafili, L., Gharib, M., Morsali, A., Weingart, O., and Janiak, C. (2020). Coordinatively unsaturated metal sites (open metal sites) in metal–organic frameworks: design and applications. Chemical Society Reviews *49*, 2751-2798. 10.1039/C9CS00609E.
4. Chen, B., Eddaoudi, M., Reineke, T.M., Kampf, J.W., O'Keeffe, M., and Yaghi, O.M. (2000). $Cu_2(ATC)\cdot 6H_2O$: Design of Open Metal Sites in Porous Metal−Organic Crystals (ATC: 1,3,5,7-Adamantane Tetracarboxylate). Journal of the American Chemical Society *122*, 11559-11560. 10.1021/ja003159k.
5. Rogge, S.M.J., Bavykina, A., Hajek, J., Garcia, H., Olivos-Suarez, A.I., Sepúlveda-Escribano, A., Vimont, A., Clet, G., Bazin, P., Kapteijn, F., et al. (2017). Metal–organic and covalent organic frameworks as single-site catalysts. Chemical Society Reviews *46*, 3134-3184. 10.1039/C7CS00033B.
6. Dhakshinamoorthy, A., Li, Z., and Garcia, H. (2018). Catalysis and photocatalysis by metal organic frameworks. Chemical Society Reviews *47*, 8134-8172. 10.1039/C8CS00256H.
7. Wang, Y., and Wöll, C. (2018). Chemical Reactions at Isolated Single-Sites Inside Metal–Organic Frameworks. Catalysis Letters *148*, 2201-2222. 10.1007/s10562-018-2432-2.
8. Yan, Y., Yang, S., Blake, A.J., and Schröder, M. (2014). Studies on Metal–Organic Frameworks of Cu(II) with Isophthalate Linkers for Hydrogen Storage. Accounts of Chemical Research *47*, 296-307. 10.1021/ar400049h.
9. Kapelewski, M.T., Geier, S.J., Hudson, M.R., Stück, D., Mason, J.A., Nelson, J.N., Xiao, D.J., Hulvey, Z., Gilmour, E., FitzGerald, S.A., et al. (2014). M_2(*m*-dobdc) (M = Mg, Mn,

Fe, Co, Ni) Metal–Organic Frameworks Exhibiting Increased Charge Density and Enhanced H_2 Binding at the Open Metal Sites. Journal of the American Chemical Society *136*, 12119-12129. 10.1021/ja506230r.

10. Rosnes, M.H., Opitz, M., Frontzek, M., Lohstroh, W., Embs, J.P., Georgiev, P.A., and Dietzel, P.D.C. (2015). Intriguing differences in hydrogen adsorption in CPO-27 materials induced by metal substitution. Journal of Materials Chemistry A *3*, 4827-4839. 10.1039/C4TA05794E.
11. Chen, B., Ockwig, N.W., Millward, A.R., Contreras, D.S., and Yaghi, O.M. (2005). High H_2 Adsorption in a Microporous Metal–Organic Framework with Open Metal Sites. Angewandte Chemie International Edition *44*, 4745-4749. 10.1002/anie.200462787.
12. Shustova, N.B., Cozzolino, A.F., Reineke, S., Baldo, M., and Dincă, M. (2013). Selective Turn-On Ammonia Sensing Enabled by High-Temperature Fluorescence in Metal–Organic Frameworks with Open Metal Sites. Journal of the American Chemical Society *135*, 13326-13329. 10.1021/ja407778a.
13. Pentyala, V., Davydovskaya, P., Ade, M., Pohle, R., and Urban, G. (2016). Carbon dioxide gas detection by open metal site metal organic frameworks and surface functionalized metal organic frameworks. Sensors and Actuators B: Chemical *225*, 363-368. 10.1016/j.snb.2015.11.071.
14. Wuttke, S., Dietl, C., Hinterholzinger, F.M., Hintz, H., Langhals, H., and Bein, T. (2014). Turn-on fluorescence triggered by selective internal dye replacement in MOFs. Chemical Communications *50*, 3599-3601. 10.1039/C3CC46591H.
15. Marshall, R.J., McGuire, J., Wilson, C., and Forgan, R.S. (2018). Crystallographic investigation into the self-assembly, guest binding, and flexibility of urea functionalised metal-organic frameworks. Supramolecular Chemistry *30*, 732-741. 10.1080/10610278.2017.1370095.
16. Canossa, S., Pelagatti, P., and Bacchi, A. (2018). Drinking and Breathing: Solvent Coordination-driven Plasticity of IRMOF-9. Israel Journal of Chemistry *58*, 1131-1137. 10.1002/ijch.201800061.
17. Brozek, C.K., Michaelis, V.K., Ong, T.-C., Bellarosa, L., López, N., Griffin, R.G., and Dincă, M. (2015). Dynamic DMF Binding in MOF-5 Enables the Formation of Metastable Cobalt-Substituted MOF-5 Analogues. ACS Central Science *1*, 252-260. 10.1021/acscentsci.5b00247.
18. Cui, P., Wang, P., Zhao, Y., and Sun, W.-Y. (2019). Fabrication of Desired Metal–Organic Frameworks via Postsynthetic Exchange and Sequential Linker Installation. Crystal Growth & Design *19*, 1454-1470. 10.1021/acs.cgd.8b01628.

19. Karagiaridi, O., Bury, W., Mondloch, J.E., Hupp, J.T., and Farha, O.K. (2014). Solvent-Assisted Linker Exchange: An Alternative to the De Novo Synthesis of Unattainable Metal–Organic Frameworks. Angewandte Chemie International Edition *53*, 4530-4540. 10.1002/anie.201306923.
20. Deria, P., Mondloch, J.E., Karagiaridi, O., Bury, W., Hupp, J.T., and Farha, O.K. (2014). Beyond post-synthesis modification: evolution of metal–organic frameworks via building block replacement. Chemical Society Reviews *43*, 5896-5912. 10.1039/C4CS00067F.
21. Kim, M., Cahill, J.F., Su, Y., Prather, K.A., and Cohen, S.M. (2012). Postsynthetic ligand exchange as a route to functionalization of 'inert' metal–organic frameworks. Chemical Science *3*, 126-130. 10.1039/C1SC00394A.
22. Burnett, B.J., Barron, P.M., Hu, C., and Choe, W. (2011). Stepwise Synthesis of Metal–Organic Frameworks: Replacement of Structural Organic Linkers. Journal of the American Chemical Society *133*, 9984-9987. 10.1021/ja201911v.
23. Deria, P., Mondloch, J.E., Tylianakis, E., Ghosh, P., Bury, W., Snurr, R.Q., Hupp, J.T., and Farha, O.K. (2013). Perfluoroalkane Functionalization of NU-1000 via Solvent-Assisted Ligand Incorporation: Synthesis and CO_2 Adsorption Studies. Journal of the American Chemical Society *135*, 16801-16804. 10.1021/ja408959g.
24. Deria, P., Bury, W., Hupp, J.T., and Farha, O.K. (2014). Versatile functionalization of the NU-1000 platform by solvent-assisted ligand incorporation. Chemical Communications *50*, 1965-1968. 10.1039/C3CC48562E.
25. Hwang, Y.K., Hong, D.-Y., Chang, J.-S., Jhung, S.H., Seo, Y.-K., Kim, J., Vimont, A., Daturi, M., Serre, C., and Férey, G. (2008). Amine Grafting on Coordinatively Unsaturated Metal Centers of MOFs: Consequences for Catalysis and Metal Encapsulation. Angewandte Chemie International Edition *47*, 4144-4148. 10.1002/anie.200705998.
26. McDonald, T.M., Mason, J.A., Kong, X., Bloch, E.D., Gygi, D., Dani, A., Crocellà, V., Giordanino, F., Odoh, S.O., Drisdell, W.S., et al. (2015). Cooperative insertion of CO_2 in diamine-appended metal-organic frameworks. Nature *519*, 303-308. 10.1038/nature14327.
27. Yan, J., MacDonald, J.C., Maag, A.R., Coudert, F.-X., and Burdette, S.C. (2019). MOF Decomposition and Introduction of Repairable Defects Using a Photodegradable Strut. Chemistry – A European Journal *25*, 8393-8400. 10.1002/chem.201901213.
28. Gutov, O.V., Hevia, M.G., Escudero-Adán, E.C., and Shafir, A. (2015). Metal–Organic Framework (MOF) Defects under Control: Insights into the Missing Linker Sites and Their Implication in the Reactivity of Zirconium-Based Frameworks. Inorganic Chemistry *54*, 8396-8400. 10.1021/acs.inorgchem.5b01053.

29. Wang, X., Zhai, L., Wang, Y., Li, R., Gu, X., Yuan, Y.D., Qian, Y., Hu, Z., and Zhao, D. (2017). Improving Water-Treatment Performance of Zirconium Metal-Organic Framework Membranes by Postsynthetic Defect Healing. ACS Applied Materials & Interfaces *9*, 37848-37855. 10.1021/acsami.7b12750.
30. Park, H., Kim, S., Jung, B., Park, M.H., Kim, Y., and Kim, M. (2018). Defect Engineering into Metal–Organic Frameworks for the Rapid and Sequential Installation of Functionalities. Inorganic Chemistry *57*, 1040-1047. 10.1021/acs.inorgchem.7b02391.
31. Shearer, G.C., Vitillo, J.G., Bordiga, S., Svelle, S., Olsbye, U., and Lillerud, K.P. (2016). Functionalizing the Defects: Postsynthetic Ligand Exchange in the Metal Organic Framework UiO-66. Chemistry of Materials *28*, 7190-7193. 10.1021/acs.chemmater.6b02749.
32. Taddei, M., Wakeham, R.J., Koutsianos, A., Andreoli, E., and Barron, A.R. (2018). Post-Synthetic Ligand Exchange in Zirconium-Based Metal–Organic Frameworks: Beware of The Defects! Angewandte Chemie International Edition *57*, 11706-11710. 10.1002/anie.201806910.
33. Karagiaridi, O., Vermeulen, N.A., Klet, R.C., Wang, T.C., Moghadam, P.Z., Al-Juaid, S.S., Stoddart, J.F., Hupp, J.T., and Farha, O.K. (2015). Functionalized Defects through Solvent-Assisted Linker Exchange: Synthesis, Characterization, and Partial Postsynthesis Elaboration of a Metal–Organic Framework Containing Free Carboxylic Acid Moieties. Inorganic Chemistry *54*, 1785-1790. 10.1021/ic502697y.
34. Cychosz, K.A., and Matzger, A.J. (2010). Water Stability of Microporous Coordination Polymers and the Adsorption of Pharmaceuticals from Water. Langmuir *26*, 17198-17202. 10.1021/la103234u.
35. Giovine, R., Volkringer, C., Ashbrook, S.E., Trébosc, J., McKay, D., Loiseau, T., Amoureux, J.-P., Lafon, O., and Pourpoint, F. (2017). Solid-State NMR Spectroscopy Proves the Presence of Penta-coordinated Sc Sites in MIL-100(Sc). Chemistry – A European Journal *23*, 9525-9534. 10.1002/chem.201700584.
36. Ahmed, I., Mondol, M.M.H., Jung, M.J., Lee, G.H., and Jhung, S.H. (2023). MOFs with bridging or terminal hydroxo ligands: Applications in adsorption, catalysis, and functionalization. Coordination Chemistry Reviews *475*, 214912. 10.1016/j.ccr.2022.214912.
37. Ashbrook, S.E., Davis, Z.H., Morris, R.E., and Rice, C.M. (2021). ^{17}O NMR spectroscopy of crystalline microporous materials. Chemical Science *12*, 5016-5036. 10.1039/D1SC00552A.

38. Bignami, G.P.M., Davis, Z.H., Dawson, D.M., Morris, S.A., Russell, S.E., McKay, D., Parke, R.E., Iuga, D., Morris, R.E., and Ashbrook, S.E. (2018). Cost-effective ^{17}O enrichment and NMR spectroscopy of mixed-metal terephthalate metal–organic frameworks. Chemical Science *9*, 850-859. 10.1039/C7SC04649A.
39. Pugh, S.M., Wright, P.A., Law, D.J., Thompson, N., and Ashbrook, S.E. (2020). Facile, Room-Temperature ^{17}O Enrichment of Zeolite Frameworks Revealed by Solid-State NMR Spectroscopy. Journal of the American Chemical Society *142*, 900-906. 10.1021/jacs.9b10528.
40. Bignami, G.P.M., Dawson, D.M., Seymour, V.R., Wheatley, P.S., Morris, R.E., and Ashbrook, S.E. (2017). Synthesis, Isotopic Enrichment, and Solid-State NMR Characterization of Zeolites Derived from the Assembly, Disassembly, Organization, Reassembly Process. Journal of the American Chemical Society *139*, 5140-5148. 10.1021/jacs.7b00386.
41. Boutin, A., Bousquet, D., Ortiz, A.U., Coudert, F.-X., Fuchs, A.H., Ballandras, A., Weber, G., Bezverkhyy, I., Bellat, J.-P., Ortiz, G., et al. (2013). Temperature-Induced Structural Transitions in the Gallium-Based MIL-53 Metal–Organic Framework. The Journal of Physical Chemistry C *117*, 8180-8188. 10.1021/jp312179e.
42. Liu, L., Wang, X., and Jacobson, A.J. (2010). AlF·1,4-benzenedicarboxylate: synthesis and absorption properties. Dalton Transactions *39*, 1722-1725. 10.1039/B919161E.
43. Nanthamathee, C., Ling, S., Slater, B., and Attfield, M.P. (2015). Contradistinct Thermoresponsive Behavior of Isostructural MIL-53 Type Metal–Organic Frameworks by Modifying the Framework Inorganic Anion. Chemistry of Materials *27*, 85-95. 10.1021/cm503311x.
44. Bara, D., Meekel, E.G., Pakamorė, I., Wilson, C., Ling, S., and Forgan, R.S. (2021). Exploring and expanding the Fe-terephthalate metal–organic framework phase space by coordination and oxidation modulation. Materials Horizons *8*, 3377-3386. 10.1039/D1MH01663F.
45. Munn, A.S., Clarkson, G.J., Millange, F., Dumont, Y., and Walton, R.I. (2013). M(II) (M = Mn, Co, Ni) variants of the MIL-53-type structure with pyridine-N-oxide as a co-ligand. CrystEngComm *15*, 9679-9687. 10.1039/C3CE41268G.
46. Whitfield, T.R., Wang, X., Liu, L., and Jacobson, A.J. (2005). Metal-organic frameworks based on iron oxide octahedral chains connected by benzenedicarboxylate dianions. Solid State Sciences *7*, 1096-1103. 10.1016/j.solidstatesciences.2005.03.007.
47. Thom, A.J.R., Madden, D.G., Bueno-Perez, R., Al Shakhs, A.N., Lennon, C.T., Marshall, R.J., Walshe, C.A., Wilson, C., Murray, C.A., Thompson, S.P., et al. (2022). Modulated

self-assembly of an interpenetrated MIL-53 Sc metal–organic framework with excellent volumetric H_2 storage and working capacity. Materials Today Chemistry *24*, 100887. 10.1016/j.mtchem.2022.100887.

48. McKellar, S.C., Graham, A.J., Allan, D.R., Mohideen, M.I.H., Morris, R.E., and Moggach, S.A. (2014). The effect of pressure on the post-synthetic modification of a nanoporous metal–organic framework. Nanoscale *6*, 4163-4173. 10.1039/C3NR04161A.
49. Chen, L., Mowat, J.P.S., Fairen-Jimenez, D., Morrison, C.A., Thompson, S.P., Wright, P.A., and Düren, T. (2013). Elucidating the Breathing of the Metal–Organic Framework MIL-53(Sc) with ab Initio Molecular Dynamics Simulations and in Situ X-ray Powder Diffraction Experiments. Journal of the American Chemical Society *135*, 15763-15773. 10.1021/ja403453g.
50. Mowat, J.P.S., Seymour, V.R., Griffin, J.M., Thompson, S.P., Slawin, A.M.Z., Fairen-Jimenez, D., Düren, T., Ashbrook, S.E., and Wright, P.A. (2012). A novel structural form of MIL-53 observed for the scandium analogue and its response to temperature variation and CO_2 adsorption. Dalton Transactions *41*, 3937-3941. 10.1039/C1DT11729G.
51. McKellar, S.C., and Moggach, S.A. (2015). Structural studies of metal-organic frameworks under high pressure. Acta Crystallographica Section B *71*, 587-607. 10.1107/S2052520615018168.
52. Hobday, C.L., Marshall, R.J., Murphie, C.F., Sotelo, J., Richards, T., Allan, D.R., Düren, T., Coudert, F.-X., Forgan, R.S., Morrison, C.A., et al. (2016). A Computational and Experimental Approach Linking Disorder, High-Pressure Behavior, and Mechanical Properties in UiO Frameworks. Angewandte Chemie International Edition *55*, 2401-2405. 10.1002/anie.201509352.
53. Graham, A.J., Allan, D.R., Muszkiewicz, A., Morrison, C.A., and Moggach, S.A. (2011). The Effect of High Pressure on MOF-5: Guest-Induced Modification of Pore Size and Content at High Pressure. Angewandte Chemie International Edition *50*, 11138-11141. 10.1002/anie.201104285.
54. Iacomi, P., Lee, J.S., Vanduyfhuys, L., Cho, K.H., Fertey, P., Wieme, J., Granier, D., Maurin, G., Van Speybroeck, V., Chang, J.-S., and Yot, P.G. (2021). Crystals springing into action: metal–organic framework CUK-1 as a pressure-driven molecular spring. Chemical Science *12*, 5682-5687. 10.1039/D1SC00205H.
55. McMonagle, C.J., Comar, P., Nichol, G.S., Allan, D.R., González, J., Barreda-Argüeso, J.A., Rodríguez, F., Valiente, R., Turner, G.F., Brechin, E.K., and Moggach, S.A. (2020). Pressure-and temperature induced phase transitions, piezochromism, NLC behaviour and

pressure controlled Jahn–Teller switching in a Cu-based framework. Chemical Science *11*, 8793-8799. 10.1039/D0SC03229H.

56. Turner, G.F., McKellar, S.C., Allan, D.R., Cheetham, A.K., Henke, S., and Moggach, S.A. (2021). Guest-mediated phase transitions in a flexible pillared-layered metal–organic framework under high-pressure. Chemical Science *12*, 13793-13801. 10.1039/D1SC03108B.
57. Yan, Y., O'Connor, A.E., Kanthasamy, G., Atkinson, G., Allan, D.R., Blake, A.J., and Schröder, M. (2018). Unusual and Tunable Negative Linear Compressibility in the Metal–Organic Framework MFM-133(M) (M = Zr, Hf). Journal of the American Chemical Society *140*, 3952-3958. 10.1021/jacs.7b11747.
58. Sussardi, A., Hobday, C.L., Marshall, R.J., Forgan, R.S., Jones, A.C., and Moggach, S.A. (2020). Correlating Pressure-Induced Emission Modulation with Linker Rotation in a Photoluminescent MOF. Angewandte Chemie International Edition *59*, 8118-8122. 10.1002/anie.202000555.
59. Sussardi, A., Marshall, R.J., Moggach, S.A., Jones, A.C., and Forgan, R.S. (2021). Photophysics of Azobenzene Constrained in a UiO Metal–Organic Framework: Effects of Pressure, Solvation and Dynamic Disorder. Chemistry – A European Journal *27*, 14871-14875. 10.1002/chem.202101879.
60. Macrae, C.F., Sovago, I., Cottrell, S.J., Galek, P.T.A., McCabe, P., Pidcock, E., Platings, M., Shields, G.P., Stevens, J.S., Towler, M., and Wood, P.A. (2020). Mercury 4.0: from visualization to analysis, design and prediction. Journal of Applied Crystallography *53*, 226-235. 10.1107/S1600576719014092.
61. Moggach, S.A., Allan, D.R., Parsons, S., and Warren, J.E. (2008). Incorporation of a new design of backing seat and anvil in a Merrill-Bassett diamond anvil cell. Journal of Applied Crystallography *41*, 249-251. 10.1107/S0021889808000514.
62. Spek, A. (2015). PLATON SQUEEZE: a tool for the calculation of the disordered solvent contribution to the calculated structure factors. Acta Crystallographica Section C *71*, 9-18. 10.1107/S2053229614024929.
63. Spek, A. (2003). Single-crystal structure validation with the program PLATON. Journal of Applied Crystallography *36*, 7-13. 10.1107/S0021889802022112.
64. Ortiz, A.U., Boutin, A., Fuchs, A.H., and Coudert, F.-X. (2012). Anisotropic Elastic Properties of Flexible Metal-Organic Frameworks: How Soft are Soft Porous Crystals? Physical Review Letters *109*, 195502. 10.1103/PhysRevLett.109.195502.
65. Serra-Crespo, P., Dikhtiarenko, A., Stavitski, E., Juan-Alcañiz, J., Kapteijn, F., Coudert, F.-X., and Gascon, J. (2015). Experimental evidence of negative linear compressibility in the

MIL-53 metal–organic framework family. CrystEngComm *17*, 276-280. 10.1039/C4CE00436A.

66. Reinsch, H., Pillai, R.S., Siegel, R., Senker, J., Lieb, A., Maurin, G., and Stock, N. (2016). Structure and properties of Al-MIL-53-ADP, a breathing MOF based on the aliphatic linker molecule adipic acid. Dalton Transactions *45*, 4179-4186. 10.1039/C5DT03510D.
67. Serra-Crespo, P., Gobechiya, E., Ramos-Fernandez, E.V., Juan-Alcañiz, J., Martinez-Joaristi, A., Stavitski, E., Kirschhock, C.E.A., Martens, J.A., Kapteijn, F., and Gascon, J. (2012). Interplay of Metal Node and Amine Functionality in NH_2-MIL-53: Modulating Breathing Behavior through Intra-framework Interactions. Langmuir *28*, 12916-12922. 10.1021/la302824j.
68. Hutchison, I.B., Delori, A., Wang, X., Kamenev, K.V., Urquhart, A.J., and Oswald, I.D.H. (2015). Polymorphism of a polymer precursor: metastable glycolide polymorph recovered via large scale high-pressure experiments. CrystEngComm *17*, 1778-1782. 10.1039/C5CE00119F.
69. Marshall, R.J., Hobday, C.L., Murphie, C.F., Griffin, S.L., Morrison, C.A., Moggach, S.A., and Forgan, R.S. (2016). Amino acids as highly efficient modulators for single crystals of zirconium and hafnium metal–organic frameworks. Journal of Materials Chemistry A *4*, 6955-6963. 10.1039/C5TA10401G.
70. Marreiros, J., Caratelli, C., Hajek, J., Krajnc, A., Fleury, G., Bueken, B., De Vos, D.E., Mali, G., Roeffaers, M.B.J., Van Speybroeck, V., and Ameloot, R. (2019). Active Role of Methanol in Post-Synthetic Linker Exchange in the Metal–Organic Framework UiO-66. Chemistry of Materials *31*, 1359-1369. 10.1021/acs.chemmater.8b04734.
71. DeCoste, J.B., Peterson, G.W., Jasuja, H., Glover, T.G., Huang, Y.-g., and Walton, K.S. (2013). Stability and degradation mechanisms of metal–organic frameworks containing the $Zr_6O_4(OH)_4$ secondary building unit. Journal of Materials Chemistry A *1*, 5642-5650. 10.1039/C3TA10662D.
72. Yang, D., Chheda, S., Lyu, Y., Li, Z., Xiao, Y., Siepmann, J.I., Gagliardi, L., and Gates, B.C. (2022). Mechanism of Methanol Dehydration Catalyzed by Al_8O_{12} Nodes Assisted by Linker Amine Groups of the Metal–Organic Framework CAU-1. ACS Catalysis *12*, 12845-12859. 10.1021/acscatal.2c01746.
73. Warfsmann, J., Tokay, B., and Champness, N.R. (2018). Synthesis of hydrophobic MIL-53(Al) nanoparticles in low molecular weight alcohols: systematic investigation of solvent effects. CrystEngComm *20*, 4666-4675. 10.1039/C8CE00913A.
74. Zhang, Y., Lucier, B.E.G., McKenzie, S.M., Arhangelskis, M., Morris, A.J., Friščić, T., Reid, J.W., Terskikh, V.V., Chen, M., and Huang, Y. (2018). Welcoming Gallium- and

Indium-Fumarate MOFs to the Family: Synthesis, Comprehensive Characterization, Observation of Porous Hydrophobicity, and CO_2 Dynamics. ACS Applied Materials & Interfaces *10*, 28582-28596. 10.1021/acsami.8b08562.